ADVANCED MATERIALS INTERFACES

www.advmatinterfaces.de

Ultrapermeable Thin Film ZIF-8/Polyamide Membrane for H_2/CO_2 Separation at High Temperature without Using Sweep Gas

*Javier Sánchez-Laínez, Lorena Paseta, Marta Navarro, Beatriz Zornoza, Carlos Téllez, and Joaquín Coronas**

The use of thin film composites containing metal–organic frameworks (MOFs) as filler is of widespread interest for nanofiltration issues, since their thin selective layer allows a high permeation flow. The application of this kind of membranes for gas separation should provide a better permeance in comparison with other polymeric membranes and a reduction in the amount of MOF required for their fabrication. Here, the preparation of 50–100 nm thick polyamide flat membranes containing zeolitic imidazolate framework-8 (ZIF-8) nanoparticles is shown via interfacial polymerization, containing a lower amount of MOF (0.013 g m^{-2} membrane) as compared to other membranes used for gas separation. The membranes are applied for H_2/CO_2 separation at high temperatures and pressures, showing a stable performance at 180 °C for at least seven days. Outstanding separation values are 328 GPU of H_2 and a H_2/CO_2 selectivity of 18.1 at 180 °C and 6 bar feed without transmembrane pressure. These membranes, also measurable without sweep gas, are highly suitable for industrial application.

1. Introduction

Carbon capture and storage *via* pre-combustion processes involves the separation of H_2/CO_2 mixtures with a high CO_2 concentration (≈45 vol%) at elevated pressure (15–20 bar) and temperature (190–210 °C).[1] However, there is a considerable concern about the high costs of these processes.[2] Membrane technology is an efficient approach for this gas separation thanks to its simplicity, ease of operation and versatility for a large number of potential uses. Although polymeric membranes rule the commercial scene for CO_2 capture, their well-known trade-off between permeability and selectivity makes it difficult to manufacture commercially attractive membranes.[3]

J. Sánchez-Laínez, L. Paseta, Dr. M. Navarro, Dr. B. Zornoza, Prof. C. Téllez, Prof. J. Coronas
Chemical and Environmental Engineering Department
Instituto de Nanociencia de Aragón(INA)
Universidad de Zaragoza
50018, Zaragoza, Spain
E-mail: coronas@unizar.es

The ORCID identification number(s) for the author(s) of this article can be found under https://doi.org/10.1002/admi.201800647.

DOI: 10.1002/admi.201800647

Thin film composite (TFC) membranes consist of an ultrathin dense polymeric layer (thicknesses generally below 100 nm)[4,5] supported on a porous support. Several techniques have been applied to fabricate multilayer composites, such as solution casting, dip-coating, spin-coating, chemical vapor deposition, and interfacial polymerization.[6] Interfacial polymerization (IP) involves the polycondensation of two multifunctional monomers that are initially dissolved in different phases (aqueous and organic solvent). When both solutions make contact, a fast polymerization reaction occurs in the interphase, making the polymer precipitate and forming a dense thin film.[7]

The combination of high water flux and salt rejection, a result of the extremely thin selective polyamide (PA) layers, has led to the successful implementation of TFC membranes in large-scale industrial processes, especially in reverse osmosis and nanofiltration.[8] Some applications in gas separation processes can also be found in the literature, and TFC membranes prepared by IP have already been applied in CO_2 separation.[9–11] Regarding H_2/CO_2 separation, Ali et. al. developed thin skin membranes by interfacial polymerization, able to achieve a H_2 permeance of 500 GPU and a H_2/CO_2 selectivity of 50.[12] However, these membranes could only withstand temperatures up to 140 °C due to the use of polysulfone supports, and precombustion capture needs membranes produced from materials with a high mechanical and thermal stability due to the harsh operating conditions involved.

The incorporation of inorganic nanoparticles into TFC membranes gave rise to the so-called thin film nanocomposite (TFN) membranes.[13] These membranes have been widely developed for nanofiltration,[14] but the research into gas separation found in the literature to date is very scarce.[15] ZIF-8 may be a perfect filler to enhance the gas separation properties of the polyamide, since TFN membranes can be considered as supported ultrathin mixed matrix membranes (MMMs), in which these fillers have already been successfully used.[16–23] ZIF-8 is a zeolitic imidazolate framework (a subfamily of the so called metal–organic frameworks, MOFs) with **sod** zeolitic topology and cavities of 1.16 nm connected through smaller windows of 0.34 nm.[24] In addition, Hess et. al. were able to prepare

ZIF-8-poly(ether sulfone) (PES) composites with a selective layer thickness of about 5 μm that showed at room temperature a H_2 permeance of 1167 ± 785 GPU and a H_2/CO_2 selectivity of 9.3 ± 3.1.[25]

This work focuses on the preparation of polyamide-based TFN membranes on polyimide P84® asymmetric supports via the IP route. These membranes incorporate several loadings of ZIF-8, forming defect-free composites that show an extraordinary H_2/CO_2 gas separation performance at significantly high temperatures (250 °C), never before achieved with this particular type of membrane. Coating the membranes with polydimethylsiloxane (PDMS) allows keeping the gas separation performance stable for seven days, preventing the damage of the polyamide layer. TFN membranes represent a real opportunity to reduce the gas separation membrane cost to ≈US$50 per m^2 by using supports industrially available for reverse osmosis and nanofiltration.[26]

2. Results

2.1. Membrane Preparation and Characterization

TFC and ZIF-8-containing TFN membranes were synthesized by IP of polyamide on P84® asymmetric porous supports prepared following the phase inversion method. **Figure 1**a shows the scanning electron microscopy (SEM) images of the cross-section of a TFC membrane. The P84® support has a thickness of around 120 μm and is constituted by two different porous layers, finger-like macropores and a ≈26 μm thick porous sponge-like layer above them. The thickness of the top layer of polyamide was not easy to distinguish from the spongy polyimide zone (see below). The TFC membrane surface (Figure 1b) reveals the typical "ridge and valley" morphology of the polyamide (PA) layer, with a continuous morphology in the absence of visible defects. SEM images were also taken of TFN membranes containing different loadings of ZIF-8 from 0.2 to 0.8% w/v (see Figure S1 in the Supporting Information). The PA layer is well formed in the presence of the ZIF-8 nanoparticles but its morphology changes as the dense and smoother areas in combination with the "ridge and valley" morphologies become more frequent. This suggests that the introduction of the filler influenced the PA layer formation. Nevertheless, the concentration of the filler in the TFN membrane is very low, which hinders the detection of the ZIF-8 nanoparticles (≈30 nm as shown in Figure S2 in the Supporting Information) by this technique, whether using surface or cross-section images. In consequence, energy-dispersive X-ray spectroscopy (EDX) analysis was used to detect Zn (weight and atomic composition) in the cross-section images of TFN membranes with 0.2% and 0.4% w/v of ZIF-8 nanoparticles (Figure 1c; Figure S3, Supporting Information). The discrepancy between the nominal loading of the membranes (% w/v) and the actual amount of Zn detected is due to the fact that the first value is referred to the amount of ZIF-8 incorporated in the reaction medium during the interfacial polymerization. Only a part of this amount was effectively incorporated into the membrane. The presence of crystalline ZIF-8 nanoparticles was demonstrated by electron diffraction of the composite PA layer. Figure 1d,e shows schemes of the ZIF-8 and a TFN membrane for a better visualization and understanding of the prepared membranes.

To study the layout and interaction of the ZIF-8 nanoparticles and PA, a piece of TFN with 0.8% w/v of ZIF-8 was immersed in *N,N*-dimethylformamide (DMF) at room temperature for 5 min to dissolve the P84® support. The separated top PA selective layer was observed by transmission electron microscopy (TEM). Since the P84® support was not previously crosslinked, it was easily dissolved in the solvent. **Figure 2**a

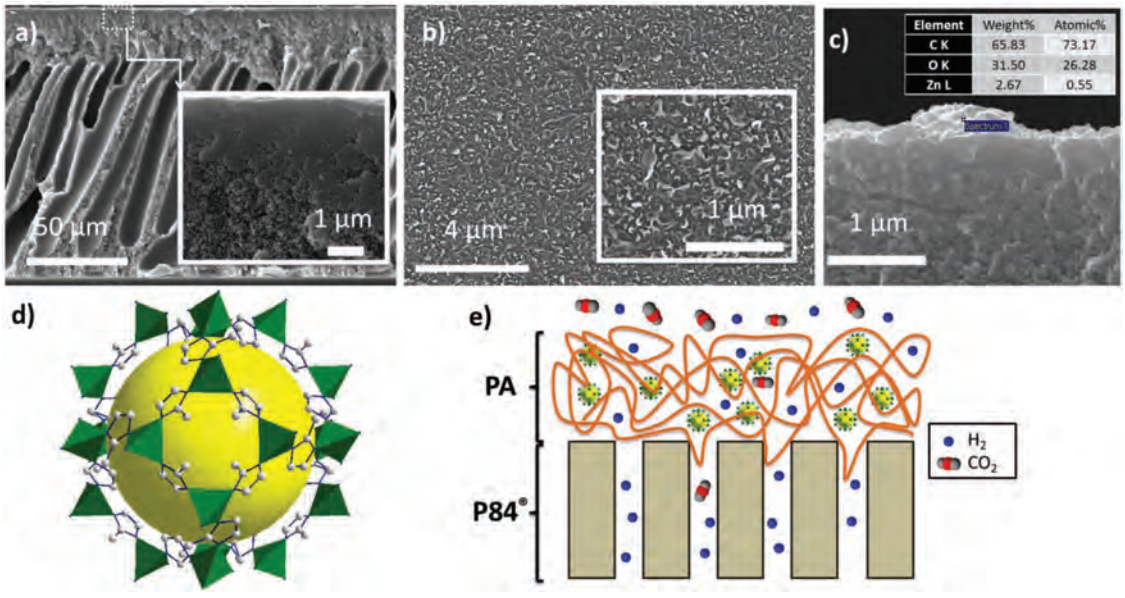

Figure 1. SEM characterization of TFCs & TFNs prepared on polyimide P84® supports. a) Image of the cross-section of a TFC with an inset at higher magnification. b) Image of the surface of the TFC with a zoom as inset. c) EDX analysis of a TFN containing a 0.8% w/v of ZIF-8. Schematic representations of d) ZIF-8 with the ZnN_4 tetrahedra in green and carbon atoms from ligand molecules in gray, and e) the TFN membrane.

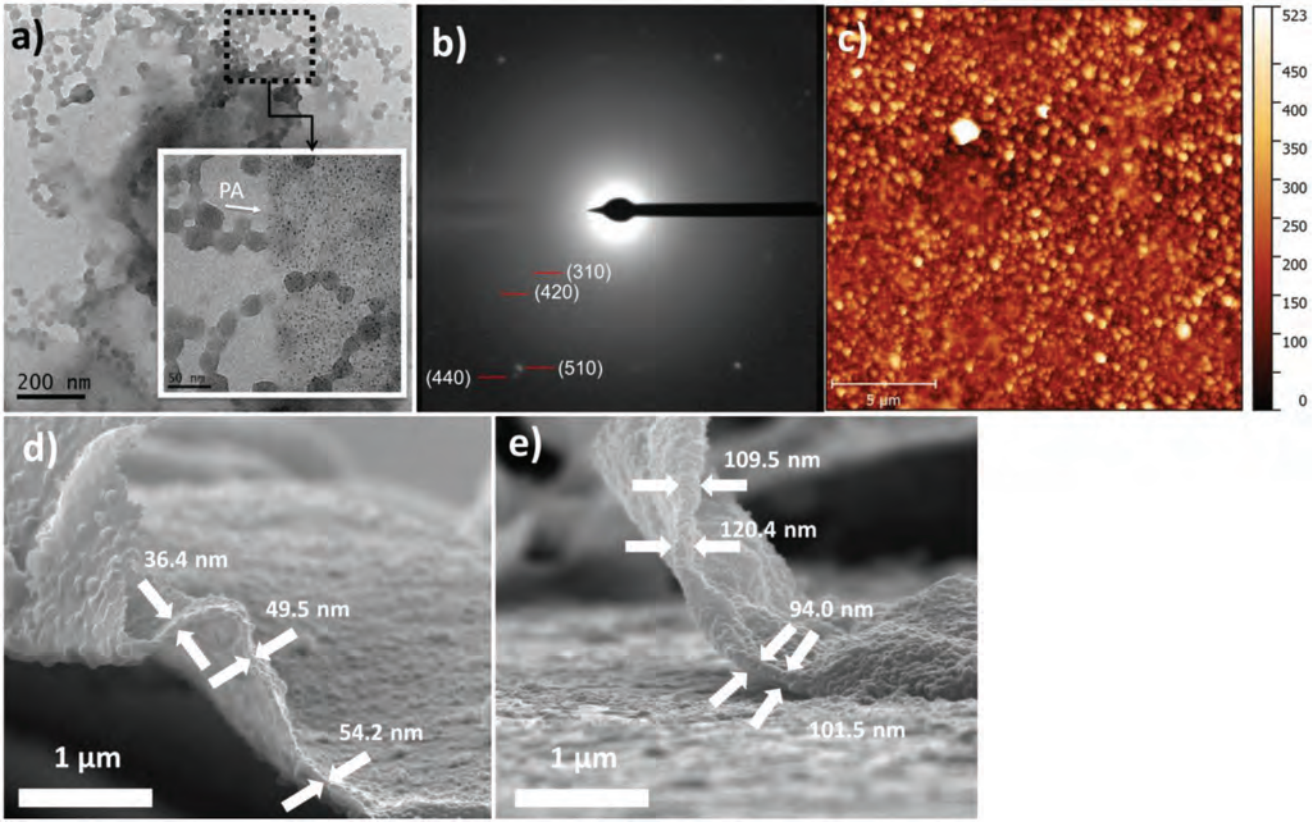

Figure 2. a) TEM image of the PA layer of a 0.8% w/v loaded TFN after the dissolution of the P84® support in DMF, with a higher magnified image as inset. b) Electron diffraction pattern in the [001] zone axis of a ZIF-8 crystal from inset (a). The diffraction spots are indicated by red lines and indexed according to the ZIF-8 crystal structure.[24] c) AFM characterization of the membrane surface of a 0.4% w/v loaded TFN with a color scale measuring the membrane roughness in nm. SEM images of the PA layer of a d) TFC and e) a TFN with 0.4% w/v of ZIF-8 nanoparticles removed from the P84® support. The arrows show the thickness of the PA layer.

illustrates small fragments of polymer with highly dispersed ZIF-8 nanoparticles embedded in them. Moreover, the electron diffraction pattern in Figure 2b of ZIF-8 in the [001] zone axis shows the spots indexed as the (310), (420), (510), and (440) diffractions consistent with the structure of ZIF-8 (*d*-spacings of 5.4, 3.8, 3.3, and 3.0 Å, respectively). The intensity of these spots was weak since the energy of the beam quickly degraded the sample. In any event, they provide evidence that the ZIF-8 structure remained unaltered during the interfacial polymerization process carried out to synthesize the TFN membrane. Moreover, Figure 2d,e shows the SEM images of the top thin PA layer detached from a TFC membrane and a TFN membrane with 0.4% w/v of ZIF-8 nanoparticles. Thicknesses of around 50 and 100 nm can be distinguished for the TFC and the TFN membranes with 0.4% v/w of ZIF-8, respectively. The thickness of the TFN is higher because of the presence of the ZIF-8 nanoparticles (again verified by EDX analysis), which can be found lodged between two sublayers of PA (see Figure S4 in the Supporting Information).

X-ray diffraction (XRD) and Fourier transform infrared spectroscopy (FTIR) analyses (Figures S5 and S6 in the Supporting Information, respectively) were also performed on TFN membranes with different loadings. Neither XRD reflections nor vibration modes of ZIF-8 were easy to distinguish, even using grazing incident diffraction (see Figure S5b in the Supporting Information). This may be because of the low concentration of the filler (maximum 0.8% w/v) dispersed in the PA membrane bulk. In any event, the XRD patterns in Figure S5 in the Supporting Information show some weak reflections at $2\theta = 9.5°$, 12.2°, and 24.8°) that may correspond to the PA layer. In the FTIR spectra in Figure S6a in the Supporting Information, two peaks related to the PA layer can be distinguished in the TFC and TFN membranes. The former at 1609 cm^{-1} corresponds to the N—H deformation vibration or C=C ring stretching vibration of the aromatic amide. The latter at 1541 cm^{-1} corresponds to the N—H in-plane bending and N—C stretching vibration of a —CO—NH— group.[27] Also, the FTIR spectra in Figure S6b in the Supporting Information show a signal at 1585 cm^{-1}, corresponding to the C=N stretching mode of the imidazole rings of mIm, the ZIF-8 linker.[28] Unfortunately, the low loading of filler makes that the accuracy of the FTIR spectra is not good enough to define the interaction between ZIF-8 and the PA. Nevertheless, physical interaction or chemical bonding cannot be discarded because of the flexibility of ZIF-8 and its partial organic nature, respectively. The TGA analysis in Figure S7 in the Supporting Information shows the thermal stabilities of all the composites. The analysis was performed under air flow (to calculate the real loading of the membranes) and N_2 flow (to simulate a reducing atmosphere similar to that present during the gas separation test). The thermograms show two

onset temperatures. The former at around 250 °C corresponds to the decomposition of the PA layer; and the latter at ≈600 °C is related to that of the P84® support. The real loading of ZIF-8 effectively incorporated in each TFN membrane was calculated to be: 0.26, 0.62, and 0.81 wt% for the 0.2, 0.4, and 0.8% w/v loadings used in the IP process, respectively. It is worth noting that these amounts correspond to the loadings of ZIF-8 with regard to the whole membrane volume, including the P84® support, and not only to the PA layer. Differential Scanning Calorimetry (DSC) analysis was also performed with the PA layer, shown in Figure S8 in the Supporting Information. Two endothermic peaks are distinguishable at 140 and 310 °C. The former may be a melting point and the latter the degradation temperature of the polymer, both usual in polyamides.[29]

The surface topography and roughness of the different membranes prepared were characterized by atomic force microscopy (AFM) and the results can be seen in Figure S9 in the Supporting Information. Each root-mean-square (RMS) roughness value was calculated from at least three images taken from 20 μm^2 of different substrates. The 0.2% w/v loaded TFN membrane presented a RMS value of 55 nm, almost double that of the TFC (RMS of 29 nm). Besides, the RMS value increased for the 0.4% w/v and 0.8% w/v TFN membranes, reaching full inhomogeneity in the latter, being 73 and 90 nm, respectively (see Figure 2c). Therefore, the increasing addition of the ZIF-8 nanoparticles, whose particle size (around 30 nm) is approximately one third of the polyamide layer thickness (Figure 2d,e), is responsible for the lower flatness of the membrane surface.

2.2. Gas Separation Performance

The TFC and the TFN membranes with ZIF-8 loadings of 0.2, 0.4, and 0.8% w/v were tested for H_2/CO_2 separation at temperatures from 35 to 250 °C and a feed pressure of 3 bar. The results are shown in the Robeson graph in **Figure 3** and also in Table S1 in the Supporting Information. Other membranes found in the literature based on ZIF-8 and tested at high temperature have also been included for comparison: ZIF-8 on P84® supports measured at 150 °C,[30] ZIF-8 on silicon nitride hollow fibers tested at 200 °C[31] and polybenzimidazole (PBI)/ZIF-8 hollow fibers measured at 180 °C.[17])

The use of a dope concentration below the critical value prevented the formation of a selective skin layer and made the films suitable for use as low resistant, non-selective supports.[33] Therefore, the P84® supports had no H_2/CO_2 selectivity. Polyimides exhibit a higher thermal and solvent resistance than polysulfone,[5,34] being more suitable for operating at the high temperatures necessary for H_2/CO_2 separation under industrial conditions, as explained above.

The TFC membrane showed good H_2 permeance, 99.7 GPU, at 35 °C but the selectivity remained poor (3.8). Increasing the temperature to 180 °C had an extremely positive effect on the gas separation performance. The H_2 permeance was fivefold higher and the H_2/CO_2 selectivity also increased, showing values over 500 GPU and H_2/CO_2 selectivity of 7.9. Additionally, a notable improvement in the gas separation performance was also experienced at the highest temperature tested, 250 °C. The H_2 permeance values were double than those achieved at

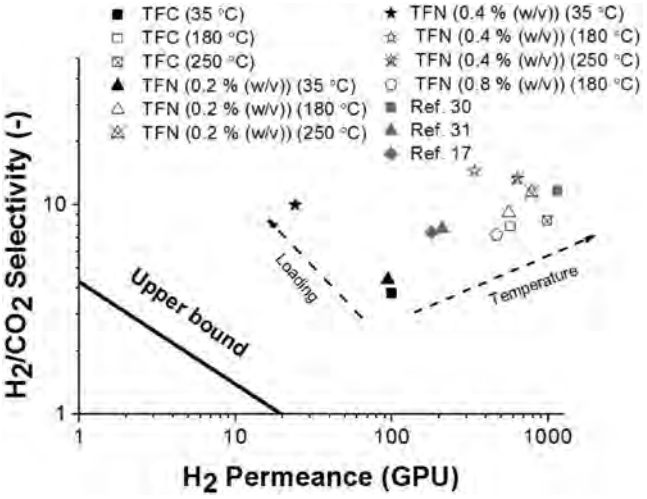

Figure 3. Gas separation performance of TFCs and TFNs at several temperatures and 3 bar feed pressure (black symbols): squares stand for TFCs; triangles for TFNs with 0.2% w/v of ZIF-8; stars for TFNs with 0.4% w/v of ZIF-8 and pentagrams for TFNs with 0.8% w/v of ZIF-8. Full symbols refer to measurements at 35 °C; crossed symbols, at 180 °C and crosses symbols, at 250 °C. The H_2/CO_2 upper bound calculated in GPU is also included[32] and bibliographical values can be seen in grey.

180 °C, being 988 GPU. There was also a 6% increase in the H_2/CO_2 selectivity, being 8.4.

Embedding ZIF-8 nanoparticles into the polyamide layer also had a positive effect on the gas separation performance. Even at the lowest temperature of 35 °C, incorporating just 0.2% w/v of ZIF-8 enhanced the gas separation performance. Besides, the H_2/CO_2 selectivity of the 0.4% w/v TFN membrane was threefold higher (10.0) than that of the TFC membrane. At 180 °C, TFNs containing 0.2% and 0.4% w/v of ZIF-8 showed respective increases in H_2/CO_2 selectivity of 42% (9.2) and 64% (14.6). However, at this high temperature, the H_2 permeance decreased as the membrane loading was higher: 338 GPU at 0.4% w/v. This is still a significantly high value for a flat membrane. The decrease in the H_2 flow may be related to the greater thickness of the PA layer as the loading of ZIF-8 increases, as already seen by SEM (see Figure 2d,e). Moreover, at the highest loading of 0.8% w/v a decrease in both permeance and selectivity could be seen. This phenomenon may be related to the defective formation of the PA layer in these TFN membranes, according to the previous characterization (see AFM results in Figure S9 in the Supporting Information), penalizing the activated and selective flow, and thus the optimum TFN membrane is observed at the intermediate 0.4% w/v loading. Raising the temperature to 250 °C led to an increase in the H_2 permeance of TFNs, but it had almost no effect on the selectivity. This may be due to defects present in the membrane related to the integration of ZIF-8 that conditions the flow at a higher temperature. It may also be due to the fact that this temperature is close to the onset temperature of the PA layer, according to the TGA and DSC analyses in Figures S7 and S8 in the Supporting Information.

The apparent activation energies of the TFC and 0.4% w/v TFN membranes were calculated for H_2 and CO_2, fitting their permeance values in Figure 3 with the Arrhenius equation

(see Figure S10 in the Supporting Information). The results in Table S2 in the Supporting Information reveal activation energies of 14.2 and 9.1 kJ mol^{-1} for H_2 and CO_2, respectively, for the TFC membrane. The TFN membrane with 0.4% w/v of ZIF-8 showed 20.6 kJ mol^{-1} for H_2 and 18.4 kJ mol^{-1} for CO_2. In line with the enhancement of gas transport through micropores, the incorporation of the ZIF nanoparticles into the polyamide layer increased the activation energy of both gases, but especially for CO_2, which almost equaled that of H_2. This fact may explain why the TFN membranes did not improve their selectivity so much with increasing temperatures, as would be expected in the case of polymeric membranes. In any event, the TFN membranes were very effective for the gas separation, even though their ZIF-8 loading was very low (below 1 wt% according to the TGA analysis shown in Figure S7 in the Supporting Information).

2.3. Membrane Stability

Although both the TFC and TFN membranes showed an outstanding H_2/CO_2 separation performance, the results were not constant when the experiment was run at 180 °C for several days. The membranes deteriorated from the first day onwards. **Figure 4**a shows the gas separation performance at 180 °C and 3 bar feed of a TFN membrane with a 0.4% w/v loading of ZIF-8, thus the optimal filler loading because it previously gave rise to the highest H_2/CO_2 selectivity at this same temperature (see Figure 3). It can be seen that the H_2 permeance of the membrane gradually increased with time while the H_2/CO_2 selectivity decreased its value. This deterioration may be due to working at an operating temperature close to the first melting point of the PA layer (see DSC analysis in Figure S8 in the Supporting Information).

In order to protect the PA layer from deteriorating, the membranes were coated with a 120 nm layer of PDMS (see Figure S11 in the Supporting Information) and tested at 180 °C for one week to check their stability. Figure 4b shows the gas separation performance of this 0.4% w/v loaded TFN membrane. The membrane was first tested under these conditions, then coated with PDMS and eventually tested again for seven days. Previous to the coating with PDMS, the membrane showed a H_2 permeance of 367 GPU and a H_2/CO_2 selectivity of 11.3. After coating, the H_2 permeance decreased to 258 GPU while the selectivity was maintained. This reduction in the H_2 flow is usual and is due to the new resistance in series added by the PDMS layer. The H_2 flow recovered during the operation time, reaching a constant value over 300 GPU after the fourth day. As the H_2/CO_2 selectivity was also stable during the whole measuring time, it can be concluded that PDMS coating sets the base for long-term stability, so that the TFN membranes may become suitable for operating under harsh conditions for long periods of time, which is industrially interesting.

The performance of the TFN membranes was also tested under different feed pressures to elucidate the influence of this variable on the gas separation performance. The results can be seen in Figure 4c. Upon increasing the feed pressure to 5 and 6 bar, the H_2 permeance increased by 5% for each pressure increase, reaching 334 GPU at 6 bar. The same occurred with the

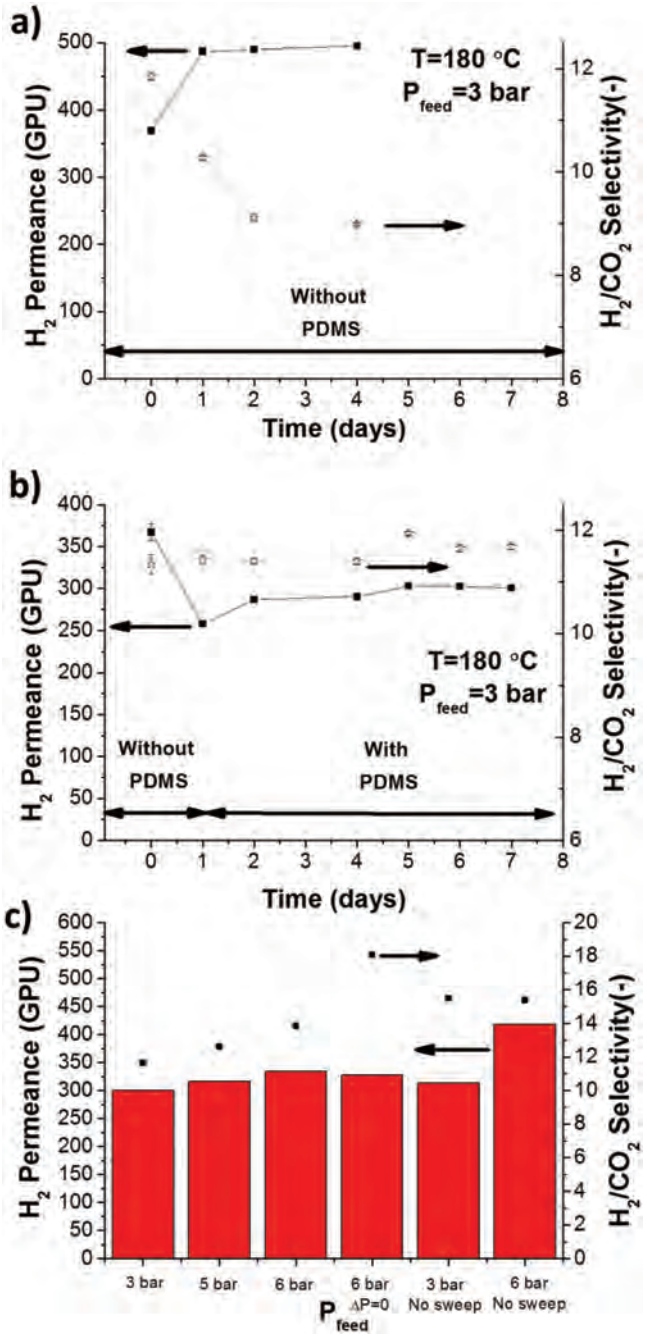

Figure 4. Gas separation performance of 0.4% w/v loaded TFN membrane. Stability test of the TFN a) without and b) with PDMS coating. The H_2 permeance (full symbols, continuous line) and H_2/CO_2 selectivity (empty symbols, dashed line) were monitored while the membrane was tested at 180 °C and 3 bar feed pressure for several days. c) Histogram of the gas separation performance of the TFN at different feed pressures: 3, 5, and 6 bar, at 6 bar feed pressure without transmembrane pressure and at 3 and 6 bar feed pressure without sweep gas. Bars refer to H_2 permeance and symbols to H_2/CO_2 selectivity.

H_2/CO_2 selectivity, which increased by 8% (13.9). Furthermore, the membranes were tested at 6 bar without transmembrane total pressure difference, setting the operating pressure at 6 bar at both the feed and the permeate side. Under these conditions,

the H_2 permeance dropped to 328 GPU, in comparison with previous values at 6 bar feed and 1 bar permeate, but the selectivity increased by 23%, reaching the highest value achieved in this work, 18.1 (Figure 4c). This enhancement may be related to the absence of viscous flow due to the lack of a total pressure gradient through the membrane. This result makes the membrane interesting for operating in cascade, since the permeate flow is obtained at high pressure, ready for the following stage. Finally, the membranes were also tested without sweep gas at 3 and 6 bar feed, showing a similar H_2 permeance and slightly higher H_2/CO_2 selectivities compared with the performance when using sweep gas (see Figure 4c). This result is of paramount importance, demonstrating the suitability of the membranes for industrial operation.

2.4. Amount of ZIF-8 for the Fabrication of Different Membranes

The amount of ZIF-8 necessary to fabricate 0.4% w/v TFN membranes, the optimal membrane loading as previously explained, has been calculated from the ZIF loading (0.62 wt% by TGA analysis) and the thickness of the membrane (150 µm). This quantity has been compared with those in other common membrane configurations in which this material has been used (see **Figure 5**). Supported ZIF-8 membranes (100% ZIF-8, thus pure MOF membranes) are the composites that need the highest amount of ZIF-8, ≈2500 g m^{-2} based on previous estimations found in the literature.[35] Using ZIF-8 in a dense mixed matrix membrane (MMM) configuration drastically reduces this amount to 9.3 g m^{-2} when the membrane has a loading of 10 wt% of ZIF.[36] As our group has recently reported,[32] when ZIF-8 is used as a filler in a membrane of the same loading but with an asymmetric configuration, the amount required was almost three times less (3.7 g m^{-2}). This reduction is related to the decrease in the skin layer thickness in comparison with dense MMMs of the same polymer. Finally, for the TFN membranes in this work, the necessary amount of filler is much lower, being only 0.013 g m^{-2}. This value is very attractive, since it would imply a significant reduction in the production cost in a hypothetical fabrication scale up. Besides, it is consistent with the 3.8 µg cm^{-2} (thus 0.038 g m^{-2}) quantified as the minimum amount of material added to the support when it is coated with a monolayer of MOF by the Langmuir–Schafer methodology.[37] The minimization of the amount of ZIF is important since all the membrane technologies designed to fight against global warming face severe economic restrictions due to the huge amounts of gases to be treated at low cost.[38] The H_2 permeance of all these membranes is also shown in Figure 5. TFN membranes show permeances 1.5 fold higher than supported membranes and 30 fold higher than asymmetric membranes, being clearly the best membrane configuration to obtain a high H_2 permeation flow. Besides, as shown above, they can selectively operate with no sweep gas, the driving force being established from a total pressure difference (5 bar).

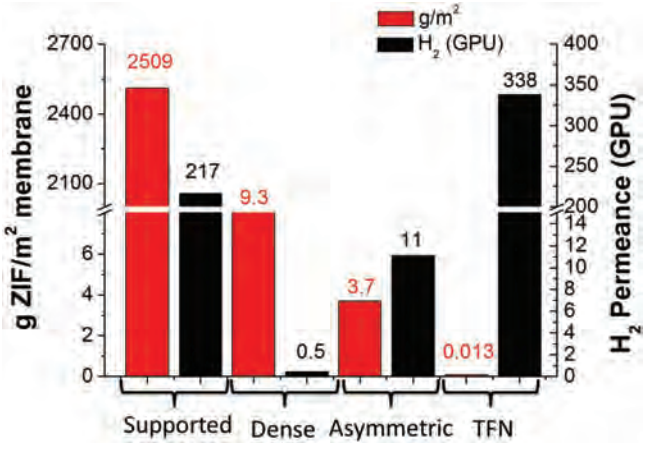

Figure 5. Histogram comparing the amount of ZIF-8 used for the membrane fabrication (red) and the H_2 permeance of the membrane (black) for: supported continuous membranes of ZIF-8 tested at 35 °C,[35] dense PBI membranes with 10 wt% of ZIF-8 tested at 180 °C,[36] asymmetric PBI membranes with 10 wt% of ZIF-8 tested at 180 °C[32] and the TFNs used in this work with 0.4% w/v of ZIF-8 tested at 180 °C.

3. Conclusion

Thin film composite membranes consisting of a selective polyamide layer on asymmetric P84® supports have been prepared in this work. ZIF-8 nanoparticles have been embedded in the polyamide matrix using different concentrations of this material from 0.2 to 0.8% w/v in the interfacial polymerization reaction medium. The polyamide layer, with a thickness between 50 and 100 nm, could be seen well formed on the membrane surfaces by SEM, with no visible defects. ZIF-8 nanoparticles were detected by TEM, where electron diffraction verified their crystallinity. FTIR also revealed weak signals of the C=N stretching mode in ZIF-8. AFM characterization showed that the membrane roughness increased with the ZIF-8 loading, until the membrane turned defective at 0.8% w/v. The membrane composites exhibited a high H_2/CO_2 separation performance at temperatures up to 250 °C. The optimal filler concentration of 0.4% w/v (real membrane loading of 0.62 wt%), produced a H_2 permeance of 338 GPU and a H_2/CO_2 selectivity of 14.6, and the high permeation flows allowed measurements without sweep gas. Coating the membranes with PDMS prevented polyamide damage, leading to membranes able to operate at high temperature during one week. The gas separation performance also improved with the feed pressure increase, especially when operating without total transmembrane pressure difference, and the H_2/CO_2 selectivity reached its maximum value (18.1). The TFN membranes could selectively operate with no sweep gas, the driving force coming from the total pressure difference (5 bar), which is important from the industrial point of view. The amount of ZIF-8 necessary to fabricate TFN membranes was calculated to be as small as 0.013 g m^{-2}, the lowest in comparison with other typical membrane configurations used for gas separation.

4. Experimental Section

Chemicals: Zinc nitrate hexahydrate ($Zn(NO_3)_2{\cdot}6H_2O$, >98%), 2-methylimidazole (mIm, $C_4H_6N_2$, >99%), trimesoyl chloride (TMC, 98%), m-phenylenediamine (MPD, 99%), and *N*,*N*-dimethylacetamide (DMAc) were purchased from Sigma Aldrich. Methanol (MeOH, HPLC grade), isopropyl alcohol (IPA, 99.5%), and n-hexane were purchased

from Scharlau. Polyimide Lenzing P84® was purchased from HP polymer GmbH and PDMS Sylgard 184, consisting of a polymer base (dimethylsiloxane, dimethylvinyl-terminated) and a hardener (dimethyl, methylhydrogen siloxane), was purchased from Dow Corning.

Synthesis of ZIF-8 Nanoparticles: ZIF-8 nanoparticles were synthesized following the method reported by Cravillon et. al.[39]: 2.93 g of zinc nitrate hexahydrate was dissolved in 200 mL of MeOH. Besides, 6.49 g of mIm was dissolved in 200 mL of MeOH, and the two solutions were mixed and stirred for 1 h. The final product was collected by centrifugation, washed once with MeOH, and dried at 110 °C overnight. The resulting nanoparticles had an average particle size of around 30 nm.

Preparation of P84® Asymmetric Supports: P84® was selected as support because it is a polymer with good mechanical and thermal stabilities, able to operate at high temperatures.[40,41] Besides, the group has previous experience in the preparation of polyamide/P84® composites for nanofiltration issues.[37] Flat asymmetric porous P84® supports were prepared following the phase inversion method. A 23 wt% dope solution of P84® was prepared dissolving the corresponding amount of powder in DMAc. This dope concentration was selected because it was found to be the optimum concentration between 15 wt% (too brittle supports) and 28 wt% (too dense supports) according to the SEM images of Figure S12 in the Supporting Information. The polymer solution was cast onto a glass plate using the Elcometer 4340 Automatic Film Applicator placed in a fume hood and set at a thickness of 250 µm. Immediately afterwards the resultant polymer sheets were immersed into a tap water bath at 25 °C for 10 min. After precipitation, the membranes were kept in a deionized (DI) water bath overnight and then rinsed with IPA in order to remove the remaining DMAc. The films were dried at 100 °C for one day prior to use.

Membrane Synthesis: TFC and TFN membranes were prepared by interfacial polymerization (IP) of polyamide on the P84® asymmetric porous supports described above. The P84® support was placed in a glass filtration holder and soaked with 30 mL of a 2% w/v solution of MPD in distilled water (i.e., 2 g of MPD for every 100 mL of water) for 2 min. Then 30 mL of a solution with 0.1% w/v of TMC in hexane and 0.2%–0.8% w/v of dispersed ZIF-8 nanoparticles (only for TFNs) was added for 1 min, followed by the addition of 10 mL of pure hexane to stop the polymerization reaction. After removing the excess, an extra 20 mL of hexane was added to remove unreacted trimesoyl chloride. The excess solution was discarded and the PA thin film was then synthesized. The remaining hexane was then washed out with 10 mL of distilled water. Finally, the membranes were soaked in DI water at 80 °C for 2 min to remove the rest of the unreacted monomers and dried at 100 °C for 18 h.

PDMS Coating: To avoid damage of the polyamide layer, the TFN membranes were healed with PDMS following a dip coating method. The coating solution was prepared mixing the PDMS polymer base and hardener with a weight ratio of 10 to 1. The mixture was added to n-hexane to obtain a 3 wt% solution. The membranes were immersed in the coating solution for 5 s and then allowed to evaporate at room temperature for 2 h. Finally, the membranes were cured in an oven at 100 °C for 18 h.

Membrane Characterization: Thermogravimetric analyses (TGA) were carried out using a Mettler Toledo TGA/STDA 851e. Samples (10 mg) placed in 70 µL alumina pans were heated in 40 mL (STP) of air or nitrogen flow from 25 to 900 °C at a heating rate of 10 °C min^{-1}. Differential Scanning Calorimetry (DSC) analysis was performed on a Mettler Toledo DSC822e. Samples (10 mg) placed in 70 µL aluminum pans were heated in 40 mL (STP) of nitrogen flow from 25 to 500 °C at a heating rate of 10 °C min^{-1}. Scanning electron microscopy (SEM) images of the MOFs and membranes were obtained using a FEI Inspect F50 model SEM, operated at 20 kV. Cross-sections of the membranes were prepared by freeze-fracturing after immersion in liquid N_2 and subsequently coated with Pt. Transmission electron microscopy (TEM) images of the MOF and PA were obtained using a FEI Tecnai T20 microscope, operated at 200 kV. A piece of membrane was immersed in DMF for 2 h until the complete dissolution of the P84® support. The layer of polyamide was then placed onto a holey carbon grid, which was allowed to dry for 48 h under ambient conditions. Fourier transform infrared spectroscopy (FTIR) was performed on the ZIF-8 powder sample and on the TFC and TFN membranes, using a Bruker Vertex 70 FTIR spectrometer equipped with a DTGS detector and a Golden Gate diamond ATR accessory. The spectra were recorded on the polyamide side by averaging 40 scans in the 4000–600 cm^{-1} wavenumber range at a resolution of 4 cm^{-1}. To detect the presence of MOF nanoparticles embedded in the polyamide layer in the TFN membranes, the spectrum of the TFC membrane was subtracted from the TFN membrane. Powder X-ray diffraction (XRD) patterns of the MOFs and MMMs were obtained with Panalytical Empyrean equipment, using CuKα radiation (λ = 1.540 Å), taking data from $2\theta = 2.5°$ to 40° at a scan rate of 0.03° s^{-1}. Atomic force microscopy (AFM) characterization was performed by means of a Veeco MultiMode 8 scanning probe microscope, in tapping mode under ambient conditions. A silicon cantilever provided by Bruker, with a force constant of 40 mN and operating at a resonant frequency of 300 kHz, was used in these experiments. Images were recorded with a scan rate of 1 Hz and an amplitude set-point lower than 1 V. After the AFM observation, the average plane roughness (R_a), the root-mean-square (RMS) and the relative surface area were obtained.

Gas Separation Analysis: The membrane samples were placed in a module consisting of two stainless steel pieces and a 316LSS macroporous disk support of 3.14 cm^2 (from Mott Co.) with a 20 µm nominal pore size, and gripped inside with silicon O-rings. The membrane was placed on the porous disk that acts as support, providing mechanical stability so that the membrane can stand the high feed pressure without breaking. The permeation module was placed in a UNE 200 Memmert oven to control the temperature of the experiments. Gas separation measurements were carried out by feeding a H_2/CO_2 equimolar mixture (25/25 $cm^3(STP)\cdot min^{-1}$) at 3–6 bar to the feed side by means of two mass-flow controllers (Alicat Scientific, MC-100CCM-D), while the permeate side of the membrane was swept with a 10–30 $cm^3(STP)\cdot min^{-1}$ mass-flow controlled stream of Ar at 1–6 bar (Alicat Scientific, MC-5CCM-D). Concentrations of H_2 and CO_2 in the outgoing streams were analyzed by an Agilent 3000A online gas microchromatograph equipped with a thermal conductivity detector. Permeances were calculated in GPU (10^{-6} $cm^3(STP)$ cm^{-2} s^{-1} $cmHg^{-1}$) once the steady-state of the exit stream was reached (for at least 3 h), and the separation selectivity was calculated as the ratio of permeances. At least 2–3 membrane samples of each type were fabricated and measured to provide the corresponding error estimations. Stability tests were performed maintaining the same flow conditions for 7 d at 180 °C. A scheme of the gas separation setup can be seen in Figure S13 in the Supporting Information.

Supporting Information

Supporting Information is available from the Wiley Online Library or from the author.

Acknowledgements

The research leading to these results has received funding from the European Union Seventh Framework Programme (FP7/2007-2013) under grant agreement no. 608490, project M4CO2. In addition, financial support from the Spanish MINECO and FEDER (MAT2016-77290-R), the Aragón Government (T05) and the ESF is gratefully acknowledged. J. S.-L. thanks the Spanish Education Ministry Program FPU2014 and L.P. the Ministry of Economy, Industry and Competitiveness Program FPI2014 for their PhD grants. All the microscopy work was done in the Laboratorio de Microscopías Avanzadas at the Instituto de Nanociencia de Aragón (LMA-INA). Finally, the authors would like to acknowledge the use of the Servicio General de Apoyo a la Investigación-SAI, Universidad de Zaragoza.

Conflict of Interest

The authors declare no conflict of interest.

Keywords

H_2/CO_2 separation, interfacial polymerization, membranes, metal–organic frameworks, polyamide

Received: April 26, 2018
Revised: June 1, 2018
Published online: July 12, 2018

[1] Z. Dai, L. Ansaloni, L. Deng, *Ind. Eng. Chem. Res.* **2016**, *55*, 5983.
[2] D. M. Reiner, *Nat. Energy* **2016**, *1*, 15011.
[3] L. M. Robeson, *J. Membr. Sci.* **2008**, *320*, 390.
[4] S. Karan, Z. Jiang, A. G. Livingston, *Science* **2015**, *348*, 1347.
[5] M. F. Jimenez-Solomon, Q. Song, K. E. Jelfs, M. Munoz-Ibanez, A. G. Livingston, *Nat. Mater.* **2016**, *15*, 760.
[6] Z. Dai, L. Ansaloni, L. Deng, *Green Energy Environ.* **2016**, *1*, 102.
[7] S. V. Joshi, A. V. Rao, *J. Appl. Polym. Sci.* **1991**, *42*, 1773.
[8] M. J. Raaijmakers, N. E. Benes, *Prog. Polym. Sci.* **2016**, *63*, 86.
[9] J. Zhao, Z. Wang, J. Wang, S. Wang, *J. Membr. Sci.* **2006**, *283*, 346.
[10] X. Yu, Z. Wang, Z. Wei, S. Yuan, J. Zhao, J. Wang, S. Wang, *J. Membr. Sci.* **2010**, *362*, 265.
[11] M. Wang, Z. Wang, S. Li, C. Zhang, J. Wang, S. Wang, *Energy Environ. Sci.* **2013**, *6*, 539.
[12] Z. Ali, F. Pacheco, E. Litwiller, Y. Wang, Y. Han, I. Pinnau, *J. Mater. Chem. A* **2018**, *6*, 30.
[13] B. Jeong, E. M. Hoek, Y. Yan, A. Subramani, X. Huang, G. Hurwitz, A. K. Ghosh, A. Jawor, *J. Membr. Sci.* **2007**, *294*, 1.
[14] S. Sorribas, P. Gorgojo, C. Tellez, J. Coronas, A. G. Livingston, *J. Am. Chem. Soc.* **2013**, *135*, 15201.
[15] S. Yu, S. Li, S. Huang, Z. Zeng, S. Cui, Y. Liu, *J. Membr. Sci.* **2017**, *540*, 155.
[16] T. Yang, T. Chung, *Int. J. Hydrogen Energy* **2013**, *38*, 229.
[17] T. Yang, G. M. Shi, T. Chung, *Adv. Energy Mater.* **2012**, *2*, 1358.
[18] A. F. Bushell, M. P. Attfield, C. R. Mason, P. M. Budd, Y. Yampolskii, L. Starannikova, A. Rebrov, F. Bazzarelli, P. Bernardo, J. Carolus Jansen, M. Lanč, K. Friess, V. Shantarovich, V. Gustov, V. Isaeva, *J. Membr. Sci.* **2013**, *427*, 48.
[19] L. Xu, L. Xiang, C. Wang, J. Yu, L. Zhang, Y. Pan, *Chin. J. Chem. Eng.* **2017**, *25*, 882.
[20] J. A. Thompson, J. T. Vaughn, N. A. Brunelli, W. J. Koros, C. W. Jones, S. Nair, *Microporous Mesoporous Mater.* **2014**, *192*, 43.
[21] S. Shahid, K. Nijmeijer, *J. Membr. Sci.* **2014**, *470*, 166.
[22] Q. Song, S. Nataraj, M. V. Roussenova, J. C. Tan, D. J. Hughes, W. Li, P. Bourgoin, M. A. Alam, A. K. Cheetham, S. A. Al-Muhtaseb, *Energy Environ. Sci.* **2012**, *5*, 8359.
[23] M. J. C. Ordonez, K. J. Balkus, Jr., J. P. Ferraris, I. H. Musselman, *J. Membr. Sci.* **2010**, *361*, 28.
[24] K. S. Park, Z. N. Ni, A. P. Côté, J. Y. Choi, R. Huang, F. J. Uribe-Romo, H. K. Chae, M. O'Keeffe, O. M. Yaghi, *PNAS* **2006**, *103*, 10186.
[25] S. C. Hess, R. N. Grass, W. J. Stark, *Chem. Mater.* **2016**, *28*, 7638.
[26] B. Ghalei, K. Sakurai, Y. Kinoshita, K. Wakimoto, A. P. Isfahani, Q. Song, K. Doitomi, S. Furukawa, H. Hirao, H. Kusuda, *Nat. Energy* **2017**, *2*, 17086.
[27] C. Y. Tang, Y. Kwon, J. O. Leckie, *Desalination* **2009**, *242*, 149.
[28] Y. Hu, H. Kazemian, S. Rohani, Y. Huang, Y. Song, *Chem. Commun.* **2011**, *47*, 12694.
[29] I. Kolesov, R. Androsch, *Polymer* **2012**, *53*, 4770.
[30] F. Cacho-Bailo, M. Etxeberria-Benavides, O. David, C. Téllez, J. Coronas, *ACS Appl. Mater. Interfaces* **2017**, *9*, 20787.
[31] J. Wang, N. Li, Z. Li, J. Wang, X. Xu, C. Chen, *Ceram. Int.* **2016**, *42*, 8949.
[32] J. Sánchez-Laínez, B. Zornoza, C. Tellez, J. Coronas, *J. Membr. Sci.* **2018**, *563*, 427.
[33] S. S. Hosseini, N. Peng, T. S. Chung, *J. Membr. Sci.* **2010**, *349*, 156.
[34] B. Zornoza, C. Téllez, J. Coronas, *J. Membr. Sci.* **2011**, *368*, 100.
[35] S. Friebe, A. Mundstock, D. Schneider, J. Caro, *Chem.-A Eur. J.* **2017**, *23*, 6522.
[36] J. Sánchez-Laínez, B. Zornoza, S. Friebe, J. Caro, S. Cao, A. Sabetghadam, B. Seoane, J. Gascon, F. Kapteijn, C. Le Guillouzer, *J. Membr. Sci.* **2016**, *515*, 45.
[37] M. Navarro, J. Benito, L. Paseta, I. Gascón, J. Coronas, C. Téllez, *ACS Appl. Mater. Interfaces* **2017**, *10*, 1278.
[38] L. Giordano, D. Roizard, E. Favre, *Int. J. Greenhouse Gas Control* **2018**, *68*, 146.
[39] J. Cravillon, S. Muenzer, S. Lohmeier, A. Feldhoff, K. Huber, M. Wiebcke, *Chem. Mater.* **2009**, *21*, 1410.
[40] F. Cacho-Bailo, G. Caro, M. Etxeberría-Benavides, O. Karvan, C. Téllez, J. Coronas, *Chem. Commun.* **2015**, *51*, 11283.
[41] F. Cacho-Bailo, I. Matito-Martos, J. Perez-Carbajo, M. Etxeberría-Benavides, O. Karvan, V. Sebastián, S. Calero, C. Téllez, J. Coronas, *Chem. Sci.* **2017**, *8*, 325.